Dichroic electron emission patterns from oriented helium ions

Niclas Wieland,[1,*] Klaus Bartschat,[2] Filippa Dudda,[1] René Wagner,[3,1] Philipp Schmidt,[3] Carlo Callegari,[4] Alexander Demidovich,[4] Giovanni De Ninno,[4] Michele Di Fraia,[4] Jiri Hofbrucker,[5] Michele Manfredda,[4] Valerija Music,[3,6,7] Oksana Plekan,[4] Kevin C. Prince,[4] Daniel E. Rivas,[3] Marco Zangrando,[4,8] Nicolas Douguet,[9] Alexei N. Grum-Grzhimailo,[10] Michael Meyer,[3] and Markus Ilchen[1,7,3]

[1]*Department of Physics, Universität Hamburg, D-22607 Hamburg, Germany*
[2]*Department of Physics and Astronomy, Drake University, Des Moines, Iowa 50311, USA*
[3]*European X-Ray Free-Electron Laser Facility, D-22869 Schenefeld, Germany*
[4]*Elettra-Sincrotrone Trieste S.C.p.A., I-34149 Basovizza, Trieste, Italy*
[5]*Helmholtz-Institut Jena, Fröbelstieg 3, D-07743 Jena, Germany*
[6]*Institut für Physik und CINSaT, Universität Kassel, D-34132 Kassel, Germany*
[7]*Deutsches Elektronen-Synchrotron DESY, Notkestrasse 85, D-22607 Hamburg, Germany*
[8]*CNR Istituto Officina dei Materiali, Laboratorio TASC, I-34149 Basovizza, Trieste, Italy*
[9]*Department of Physics, University of Central Florida, Orlando, Florida 32816, USA*
[10]*Skobeltsyn Institute of Nuclear Physics, Lomonosov Moscow State University, Moscow 119991, Russia*

(Received 6 August 2025; revised 2 December 2025; accepted 19 February 2026; published 7 April 2026)

We report a joint experimental and theoretical study using a combination of polarization-controlled free-electron-laser (FEL) and near-infrared (NIR) pulses in a synchronized two-color photoionization scheme. Excited He^+ ions, created by extreme ultraviolet (XUV) circularly polarized radiation from the XUV-FEL FERMI in the oriented $3p\,(m=+1)$ state, are exposed to circularly polarized 784-nm NIR radiation with peak intensities from 10^{12} to 10^{13} W/cm^2. The angular distribution of the ejected electrons exhibit a strong dichroism depending on the NIR intensity. While the corotating case is defined by a single path, for the counterrotating case, there are two dominant pathways whose relative strength and phase difference are determined.

DOI: 10.1103/3z51-5g8k

I. INTRODUCTION

The transfer of angular momentum from circularly polarized photons to electrons in multiphoton ionization represents a fundamental quantum process with broad implications for precision measurements, quantum control, and attosecond science [1–6]. Recent advances in free-electron-laser (FEL) technology and quantum-sensing applications have intensified interest in understanding and controlling these helicity-dependent interactions, particularly for their potential to enable novel forms of photoelectron-angular-distribution (PAD) control [7–14]. While single-photon circular dichroism (CD) is well understood through dipole selection rules, multiphoton pathways involving intense circularly polarized light may create complex interference patterns between different angular-momentum channels that depend on field intensity and helicity configuration.

Theoretical considerations predict that the partial-wave composition of photoelectrons should exhibit distinct dependencies on intensity when the multiphoton ionization (MPI) involves corotating or counterrotating photon helicities relative to the initial electronic orbital angular momentum. In corotating configurations, where photon and electron angular momenta align, the dominant photoelectron partial wave should remain intensity independent due to angular-momentum conservation constraints. Conversely, counterrotating configurations are predicted to exhibit a strong intensity dependence due to changing interference of different multiphoton pathways [9,15].

Using a two-color scheme with temporally separated pulses (500 fs delay), we prepare $He^+(3p, m = +1)$ via sequential two-photon absorption of right-circularly polarized extreme ultraviolet (XUV) radiation (75 fs FEL pulse, selection rule $\Delta m = +1$) in the same pulse and probe it with near-infrared (NIR) multiphoton ionization [9,15,16]. This decouples the state preparation from the subsequent ionization step, thereby suppressing AC-Stark distortions during preparation while maintaining full control over photon helicity and intensity. The above-threshold ionization (ATI-1) peak serves as our primary observable, requiring five NIR photons and remaining measurable across the entire intensity range studied in this work, unlike the four-photon MPI peak that shifts below threshold at moderate intensities [15], while higher-order ATIs suffer from poor statistics. We systematically map PADs of this first ATI peak across NIR intensities from 10^{12} to 10^{13} W/cm^2 for corotating and counterrotating helicity

*Contact author: niclas.wieland@uni-hamburg.de

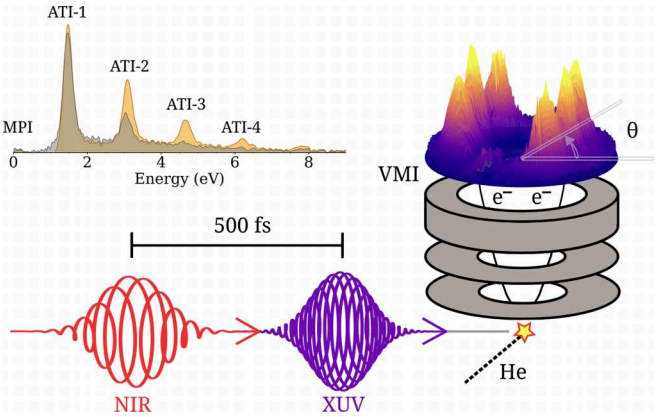

FIG. 1. Illustration of the experimental setup. Circularly polarized XUV pulses are tuned to the $3p$ resonance of He^+, which is excited by sequential two-photon absorption within the FEL pulse duration of 75 ± 25 fs [full width at half maximum (FWHM)]. After a delay of about 500 fs, circularly polarized NIR laser light with a mean photon energy of 1.58 eV (784 nm), a pulse duration of about 140 ± 30 fs (FWHM), a circular polarization of $95\% \pm 5\%$, and a bandwidth (FWHM) of 26 meV (13 nm) coaxially impinges on the sample and produces photoelectrons via absorption of several NIR photons. For a laser intensity of $\approx 1.1 \times 10^{13}$ W/cm^2, the emission spectrum (top left, gray: corotating XUV and NIR pulse; yellow: counterrotating) at the detector location of the VMI shows the ATI-1 to ATI-4 signal for co- and counterrotating fields.

configurations. For the counterrotating case, we determine both the relative strength and phase between the two dominant interfering partial-wave contributions, thereby extending the goal of performing a "complete experiment" [17] from the one-photon to the multiphoton regime.

II. EXPERIMENT

The experiments were performed at the Low-Density Matter (LDM) endstation [18] of the seeded free-electron laser FERMI [19]. For a detailed description of the laser parameters, see the caption of Fig. 1. The peak intensities of the IR laser are shifted upwards by 1.4×10^{12} W/cm^2 with respect to previously reported intensities in Ref. [15] to account for an improved understanding of the experimental conditions and in light of the theoretical findings.

In the present study, PADs were measured with a velocity-map-imaging (VMI) detector as shown in Fig. 1. For our geometry, the PAD can be fitted to the form

$$\frac{d^2\sigma}{dEd\theta}(E,\theta,I) \propto 1 + \sum_{n=2,4,6,\ldots} \beta_n(E,I)\, P_n[\cos(\theta)] \qquad (1)$$

Here, E is the ejected-electron energy, θ is the detection angle on the VMI, I is the NIR peak intensity, and $P_n[\cos(\theta)]$ denotes a standard Legendre polynomial. For $180^\circ \leqslant \theta \leqslant 360^\circ$, we use $360^\circ - \theta$ as the equivalent angle in the above formula. Experimentally, quadrant mirroring of the raw data was used to enhance the data quality. The inversion of the electron-projection data was performed with the well-established Abel algorithm [20].

Due to the symmetry of our detection scheme and the assumption that no chiral or nondipole effects play a role under the present conditions, only even-rank asymmetry parameters β_n can contribute to the sum (1). In principle, one would expect β_n to depend on both the electron energy and the peak laser intensity. However, we will see below that this dependence is not as general as one might expect at first sight.

III. THEORY

The calculations were performed with the same method and computer code described in detail by Wagner *et al.* [15] and Douguet *et al.* [21]. Briefly, we solved the time-dependent Schrödinger equation (TDSE) for the active electron starting in the $3p\,(m=+1)$ state of He^+. Due to the 500 fs delay between the generation of the excited He^+ ion, sequential ionization of the $He(1s^2)$ ground state and excitation of the remaining electron from the $1s$ to the $3p$ orbital, and the multiphoton ionization of the excited state by the intense NIR laser, this is a true one-electron problem. The nonrelativistic orbitals are known analytically, and the continuum states to project the final-state wave function on to obtain the ionization signal are pure Coulomb functions.

Without loss of generality, we assume the helicity of the XUV photon to be $+1$, i.e., we prepare the $He^+(3p, m = +1)$ state. For the corotating case, the dominant pathway after the absorption of N NIR photons, therefore, is to reach a state whose PAD is proportional to

$$\left|Y_{N+1}^{N+1}(\theta, \phi = 0^\circ, 180^\circ)\right|^2 \propto |\sin(\theta)|^{2N+2}. \qquad (2)$$

The ATI-1 line is therefore characterized by a pathway resulting in a continuum electron with angular momentum $\ell = 6$, since five NIR photons are required for the ionization process. Note that this result is entirely *independent* of the NIR intensity. Consequently, the β_n parameters cannot be independent of each other, but are the unique expansion coefficients of $|\sin(\theta)|^{2N+2}$ into a series of (orthogonal) Legendre polynomials.

IV. RESULTS AND DISCUSSION

Figure 2 shows the parameters β_n for $n = 2, 4, 6, 8$ obtained for the corotating case, i.e., the same helicity of the XUV and NIR laser beams. The validity of Eq. (2) is, indeed, verified by both the experimental data, albeit with some minor fluctuations, and the theoretical predictions. Both data sets are characterized by a constant value for the β_n parameters. We only show β_2, β_4, β_6, and β_8 for this case, even though higher terms appear but are too small to be experimentally distinguishable from zero.

Moving on to the counterrotating case, we see an entirely different pattern in Fig. 3. For this case, we experimentally determined β_2, β_4, β_6, β_8, β_{10}, and β_{12} as clearly being nonzero in general. Also, there is a strong intensity dependence for all of them, resulting in a drastic change of the PAD from the lowest intensity of 3.5×10^{12} W/cm^2 to the next selected one (5.1×10^{12} W/cm^2) and, finally, to intensities above 6×10^{12} W/cm^2. Such a strong intensity dependence of the PAD, accompanied by a rapid change over a small range of NIR intensity, was unexpected in light of the fact that (i) the

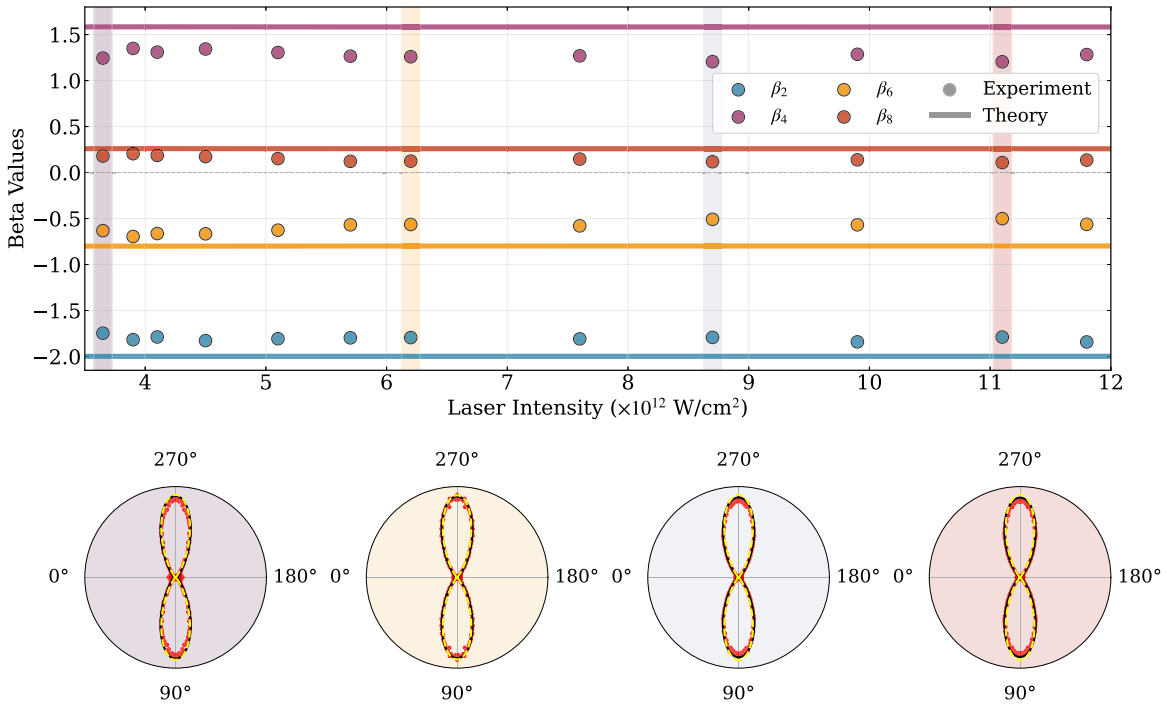

FIG. 2. Top: Beta parameters (β_2, β_4, β_6, β_8) as a function of laser intensity from 3.5 to 12×10^{12} W/cm^2 for the ATI-1 peak in the corotating case. Experimental data (solid circles) obtained by averaging over all quadrant combinations are compared with theoretical predictions (lines). Colored vertical boxes indicate the intensities selected for a detailed polar-plot analysis. Bottom: Polar plots showing PADs at four representative intensities. The red points represent the experimental data, the black solid lines show experimental fits, and the yellow dashed lines are the relative theoretical predictions. The background colors correspond to the intensity markers in the top panel.

angle-integrated dichroism (cf. Fig. 9 of Ref. [15]) is smoothly decreasing in the corresponding intensity range from about 0.4 at lowest intensity to about zero at high peak intensities and (ii) the pattern for the corotating case does not change at all.

The fact that, in contrast to the corotating case, there is an intensity dependence for the counterrotating case can be understood from the two pathways that should predominantly contribute to the PAD, namely pathways with angular momenta $\ell = 6$ and $\ell = 4$ for the outgoing electron [9]. These partial waves will interfere to form a state that can be represented by the linear combination

$$|A|Y_6^{-4} + |B| \exp(i\delta) Y_4^{-4}. \tag{3}$$

Hence, the measured angular distribution will contain the absolute strengths $|A|^2$ and $|B|^2$ that determine the generalized multiphoton cross section, as well as the interference term $|A||B| \cos\delta$. The β_n parameters then become known functions of the relative strength $|B|/|A|$ and the phase δ. Considering this, and the excellent agreement between the measured and calculated PADS (cf. Figs. 2 and 3), we refrain from further analyzing the β_n and focus on the phase δ.

It is indeed possible to determine both the relative strength and the cosine of the phase between the two dominant pathways. This two-channel model suffices here; systems with multiple comparable pathways would require additional observables or energy-resolved measurements for complete phase retrieval. Figure 4(a) shows the experimental data and the theoretical predictions for the relative strengths, normalized to their sum being 1. We see a strong intensity dependence up to intensities of about 6×10^{12} W/cm^2 with changes of the relative contributions by up to a factor of 4. Above this region of intensity, the contributions are nearly constant, with $\ell = 6$ dominating over $\ell = 4$. This is expected from the propensity rule of likely adding angular momentum to the ejected electron when its energy is increased [22]. Figure 4(b) shows $\cos(\delta)$, which also varies strongly between $+0.4$ and -0.4 in the intensity region up to 6×10^{12} W/cm^2 and then remains negative for higher intensities.

We interpret the observed patterns to originate from the crossing of the relative partial-wave strength and to the strong NIR intensity dependence of the relative phase. They *may*, at least to some extent, have to do with the fact that the MPI line moves below threshold with increasing intensity. Hence, it is more likely that the five-photon ATI-1 line is affected by the fourth photon exciting members of the dense Rydberg manifold. In this scenario, such near-resonant Rydberg states are known to cause rapid phase shifts when the ponderomotive-shifted multiphoton transitions pass through resonance at different intensities for the two paths [23], directly altering $\cos(\delta)$ and the PAD.

V. SUMMARY AND OUTLOOK

To summarize, we analyzed in detail the dichroic, angle-dependent electron-emission pattern observed after irradiating oriented $He^+(3p)$ ions, produced by circularly polarized FEL laser pulses, with intense NIR light having the same or opposite helicity as the FEL. As expected, the PAD for the corotating cases can effectively be described by a single partial wave for all intensities studied. Consequently, the

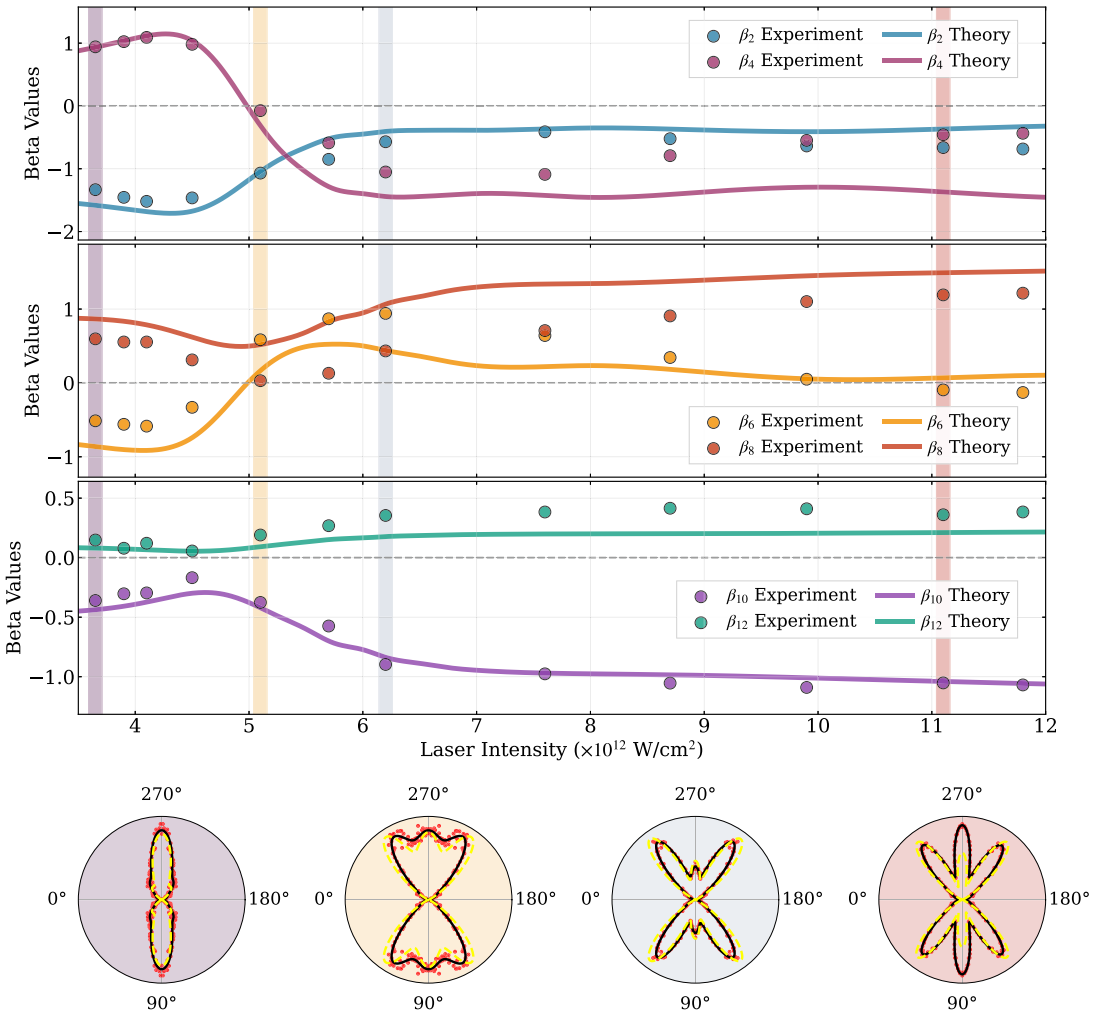

FIG. 3. Same as Fig. 2 (with expansions up to β_{12} added) for the counterrotating case. The selected angular distributions reveal a dependence on both the relative strength and the phase between the two dominant interfering pathways. The areas around 0° and 180° are affected by beam-induced artifacts. This requires the exclusion of ±15°.

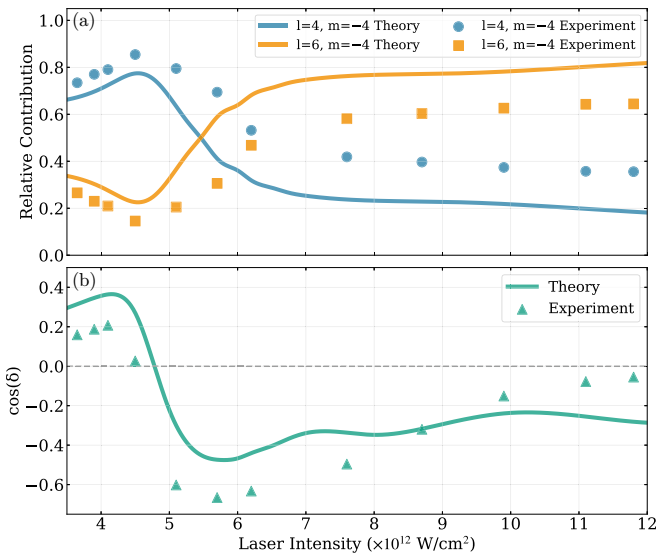

FIG. 4. (a) Dominant partial-wave contributions and (b) cos(δ) as a function of laser intensity for the ATI-1 peak in the counterrotating case.

intensity-independent β_n parameters are determined by addition theorems for the Legendre polynomials.

For the counterrotating case, on the other hand, interference of two dominating partial-wave contributions leads to more complex PADs. Interestingly, we found a rapid variation in both the relative strength and the phase as a function of the NIR intensity. Their determination brought us one step closer to a "complete experiment" in a multiphoton scenario. Realistically, however, determining the absolute values of the coefficients A and B in Eq. (3), i.e., the absolute generalized photoionization cross section, is currently out of reach.

In light of the experimental challenges, the agreement between our theoretical predictions and our experimental data is satisfactory. We suspect that less than 100% circular polarization of the two beams and slight misalignments are mainly responsible for the remaining discrepancies. We emphasize that focal-point averaging, even if it were necessary, would not resolve the differences in the corotating case, since constant β_n values are expected independent of the laser intensity.

Controlling not only the angle-integrated CD but also the angular-resolved PAD via the mutual helicity of the two laser beams and the NIR intensity is expected to be a *general* tool

that could also be applied to much more complex systems than the proof-of-principle case presented in this paper. Molecular applications, however, will require addressing competing coherent couplings between closely spaced levels.

ACKNOWLEDGMENTS

We thank Thomas Pfeifer and Christian Ott (Max Planck Institute for Nuclear Physics, Heidelberg) for fruitful discussions and the technical and scientific staff at FERMI (Elettra-Sincrotrone Trieste) for their support. R.W. and M.M. acknowledge funding by the Deutsche Forschungsgemeinschaft (DFG) in SFB-925, "Light induced dynamics and control of correlated quantum systems," Project No. 170620586. M.I., V.M., and Ph.S. received support from a Peter-Paul-Ewald Fellowship from the Volkswagen Foundation. M.I. also acknowledges DFG support under Project No. 328961117 in SFB-1319, "Extreme light for sensing and driving molecular chirality." M.I., N.W., and M.M. were supported by the DFG Cluster of Excellence "CUI: Advanced Imaging of Matter," Project No. 390715994. Theoretical work was funded by the NSF [Grants No. PHY-2408484 (K.B.) and No. PHY-2012078 (N.D.)] and the ACCESS supercomputer allocation No. PHY-090031.

DATA AVAILABILITY

The data that support the findings of this article are not publicly available upon publication because it is not technically feasible and/or the cost of preparing, depositing, and hosting the data would be prohibitive within the terms of this research project. The data are available from the authors upon reasonable request.

[1] C. Kohlfürst, Spin states in multiphoton pair production for circularly polarized light, Phys. Rev. D **99**, 096017 (2019).

[2] X. Bian and J. E. Subotnik, Angular momentum transfer between a molecular system and a continuous circularly polarized light field within a semiclassical born–oppenheimer surface hopping framework, J. Chem. Theory Comput. **20**, 6442 (2024).

[3] D. Trabert, A. Hartung, S. Eckart, F. Trinter, A. Kalinin, M. Schöffler, L. P. H. Schmidt, T. Jahnke, M. Kunitski, and R. Dörner, Spin and angular momentum in strong-field ionization, Phys. Rev. Lett. **120**, 043202 (2018).

[4] M. Ilchen, P. Schmidt, N. M. Novikovskiy, G. Hartmann, P. Rupprecht, R. N. Coffee, A. Ehresmann, A. Galler, N. Hartmann, W. Helml, *et al.*, Site-specific interrogation of an ionic chiral fragment during photolysis using an X-ray free-electron laser, Commun. Chem. **4**, 119 (2021).

[5] C. Lux, M. Wollenhaupt, C. Sarpe, and T. Baumert, Photoelectron circular dichroism of bicyclic ketones from multiphoton ionization with femtosecond laser pulses, ChemPhysChem. **16**, 115 (2015).

[6] S. Eckart, M. Kunitski, M. Richter, A. Hartung, J. Rist, F. Trinter, K. Fehre, N. Schlott, K. Henrichs, L. P. H. Schmidt, *et al.*, Ultrafast preparation and detection of ring currents in single atoms, Nat. Phys. **14**, 701 (2018).

[7] G. De Ninno, D. Gauthier, B. Mahieu, P. R. Ribič, E. Allaria, P. Cinquegrana, M. B. Danailov, A. Demidovich, E. Ferrari, L. Giannessi, G. Penco, P. Sigalotti, and M. Stupar, Single-shot spectro-temporal characterization of XUV pulses from a seeded free-electron laser, Nat. Commun. **6**, 8075 (2015).

[8] A. Karnieli, S. Tsesses, R. Yu, N. Rivera, Z. Zhao, A. Arie, S. Fan, and I. Kaminer, Quantum sensing of strongly coupled light-matter systems using free electrons, Sci. Adv. **9**, eadd2349 (2023).

[9] M. Ilchen, N. Douguet, T. Mazza, A. J. Rafipoor, C. Callegari, P. Finetti, O. Plekan, K. C. Prince, A. Demidovich, C. Grazioli, *et al.*, Circular dichroism in multiphoton ionization of resonantly excited He^+ ions, Phys. Rev. Lett. **118**, 013002 (2017).

[10] T. Mazza, M. Ilchen, A. J. Rafipoor, C. Callegari, P. Finetti, O. Plekan, K. C. Prince, R. Richter, M. B. Danailov, A. Demidovich, *et al.*, Determining the polarization state of an extreme ultraviolet free-electron laser beam using atomic circular dichroism, Nat. Commun. **5**, 3648 (2014).

[11] J. Hofbrucker, A. V. Volotka, and S. Fritzsche, Maximum elliptical dichroism in atomic two-photon ionization, Phys. Rev. Lett. **121**, 053401 (2018).

[12] M. Ilchen, E. Allaria, P. Rebernik Ribič, H.-D. Nuhn, A. Lutman, E. Schneidmiller, M. Tischer, M. Yurkov, M. Calvi, E. Prat, *et al.*, Opportunities for gas-phase science at short-wavelength free-electron lasers with undulator-based polarization control, Phys. Rev. Res. **7**, 011001 (2025).

[13] A. F. Ordonez and O. Smirnova, Disentangling enantiosensitivity from dichroism using bichromatic fields, Phys. Chem. Chem. Phys. **24**, 7264 (2022).

[14] D. Ayuso, A. F. Ordonez, and O. Smirnova, Ultrafast chirality: the road to efficient chiral measurements, Phys. Chem. Chem. Phys. **24**, 26962 (2022).

[15] R. Wagner, M. Ilchen, N. Douguet, P. Schmidt, N. Wieland, C. Callegari, Z. Delk, A. Demidovich, G. De Ninno, M. Di Fraia, *et al.*, Circular dichroism in multiphoton ionization of resonantly excited helium ions near channel closing, Sci. Rep. **14**, 27232 (2024).

[16] A. N. Grum-Grzhimailo, N. Douguet, M. Meyer, and K. Bartschat, Two-color XUV plus near-IR multiphoton near-threshold ionization of the helium ion by circularly polarized light in the vicinity of the $3p$ resonance, Phys. Rev. A **100**, 033404 (2019).

[17] N. Andersen and K. Bartschat, *Polarization, Alignment, and Orientation in Atomic Collisions*, 2nd ed. (Springer International, Cham, 2017).

[18] V. Lyamayev, Y. Ovcharenko, R. Katzy, M. Devetta, L. Bruder, A. LaForge, M. Mudrich, U. Person, F. Stienkemeier, M. Krikunova, *et al.*, A modular end-station for atomic, molecular, and cluster science at the low density matter beamline of FERMI@Elettra, J. Phys. B: At. Mol. Opt. Phys. **46**, 164007 (2013).

[19] E. Allaria, R. Appio, L. Badano, W. Barletta, S. Bassanese, S. Biedron, A. Borga, E. Busetto, D. Castronovo, P. Cinquegrana, *et al.*, Highly coherent and stable pulses from the FERMI

seeded free-electron laser in the extreme ultraviolet, Nat. Photonics **6**, 699 (2012).

[20] M. J. Vrakking, An iterative procedure for the inversion of two-dimensional ion/photoelectron imaging experiments, Rev. Sci. Instrum. **72**, 4084 (2001).

[21] N. Douguet, M. Guchkov, K. Bartschat, and S. Fonseca dos Santos, Efficient time-dependent method for strong-field ionization of atoms with smoothly varying radial steps, Atoms **12**, 34 (2024).

[22] U. Fano, Propensity rules: An analytical approach, Phys. Rev. A **32**, 617 (1985).

[23] K. Krajewska, I. I. Fabrikant, and A. F. Starace, Threshold effects in strong-field ionization: Energy shifts and Rydberg structures, Phys. Rev. A **86**, 053410 (2012).